Intrinsic ferromagnetism and restrictive thermodynamic stability in MA_2N_4 and Janus $VSiGeN_4$ monolayers

Dibyendu Dey,[1,*] Avijeet Ray,[2,†] and Liping Yu[1,‡]

[1] *Department of Physics and Astronomy, University of Maine, Orono, ME 04469, USA*
[2] *Department of Physics, Indian Institute of Technology Roorkee, Roorkee, Uttarakhand 247667, India*

The seminal experimental discovery of remarkably stable $MoSi_2N_4$ monolayer has led to a handful of predicted magnetic 2D materials in the MA_2Z_4 family (M = transition metals, A = Si, Ge, and Z = N, P, As). These magnetic monolayers were predicted to be dynamically stable, but none of them has been synthesized to date. In this work, from the first-principles thermodynamic stability analysis, we demonstrate that only the nitrides are thermodynamically stable under N-rich conditions. Based on this finding, we propose two new ferromagnetic, semiconducting Janus monolayers in the family: $VSiGeN_4$ and $VSiSnN_4$. They are both dynamically and thermally stable but only the former is further thermodynamically stable. Intriguingly, Janus $VSiGeN_4$ and $VSiSnN_4$ monolayers show weak in-plane anisotropy as compared to the VSi_2N_4 monolayer. These two emerging Janus magnetic semiconductors offer new opportunities for studying 2D magnetism and spin control for spintronics applications.

Atomically thin magnetic monolayers provide the ideal platform to study magnetism and spintronics device concepts in the two-dimensional (2D) limit, where magnetic properties can be effectively controlled or switched by proximity effects and external perturbations such as magnetic field, electric field, defects, strain, and optical doping, etc.[1–8] In the last few years, a large number of 2D intrinsic magnetic materials have been experimentally discovered and theoretically proposed.[9,10] The majority can be classified into three broad groups, namely, transition metal halides,[11,12] transition metal chalcogenides,[1,13] and MXenes and MXene analogues.[14,15] These materials have exhibited a wide spectrum of magnetic and electronic properties. However, they also carry various disadvantages for practical manufacturing applications. For example, halides and MXenes mostly are vulnerable and reactive in the presence of ambient air and water.[16,17] Besides, experimentally reported Curie temperatures (T_c) are usually much lower than the room temperature.[1,11,12] Hence, the search for new stable magnetic 2D materials continues to be a major research direction in this field.

An emerging group of 2D materials are septuple-atomic-layers of ternary transition metal pnictides in the form of MA_2Z_4, where M is the transition metal, A = Si or Ge, and Z = N, P, or As.[18] The first member of this group discovered is semiconductor $MoSi_2N_4$, centimeter-scale monolayer, which was successfully synthesized in 2020.[19] This material exhibited exceptional stability to air, water, acid, and heat. Following this discovery, first-principles calculations found tens of dynamically stable MA_2Z_4 compounds[18,20] with properties of interest for various applications such as spintronics,[21,22] superconductors,[23] and catalysts.[24,25] Of these, nine were predicted magnetic, including five nitrides (VSi_2N_4, $NbSi_2N_4$, $NbGe_2N_4$, $TaGe_2N_4$, and YSi_2N_4), two phosphides (VSi_2P_4 and VGe_2P_4), and two arsenides (VSi_2As_4 and VGe_2As_4).[18,20] Remarkably, they are all determined to be ferromagnetic and semiconducting except YSi_2N_4 which is also ferromagnetic but metallic.[20]

However, these 2D ferromagnetic MA_2Z_4 materials have yet to be synthesized. They were mainly predicted based on their dynamical stability, *ab-initio* molecular dynamics, and negative heat formation energies (meaning energetically more favorable than their constituent elemental phases). The thermodynamic stability with respect to their stable competing phases has yet to be determined. It is well known that those dynamically stable compounds can often be thermodynamically unstable and be easily decomposed into their competing phases. Such thermodynamic instability can make their experimental synthesis very challenging especially under thermodynamic (quasi-)equilibrium conditions.

Above or near room-temperature long-range magnetic ordering is necessary to realize spintronics functionality in 2D materials. Unfortunately, none of these proposed 2D ferromagnetic MA_2Z_4 compounds has been identified to possess an intrinsic long-range magnetic order with a T_c above the room temperature. For example, density functional theory (DFT) and Monte Carlo calculations suggested that monolayers VSi_2N_4 and VSi_2P_4 in the same structure as $MoSi_2N_4$ have magnetic phase transition temperatures above room temperature, but they are XY magnets.[22,26] Nevertheless, VSi_2P_4 monolayer in a different crystal structure is the only reported 2D magnet with an out-of-plane easy axis, but its predicted T_c is merely about 90 K.[18]

In this work, from the first-principles thermodynamic stability analysis (cf. supporting information S1) for all the nine 2D magnetic MA_2Z_4 monolayers, we explain why they have not been synthesized so far and suggest possible routes to grow them. 2D Janus crystals and their superlattices are a new class of 2D materials that offer extraordinary physical, chemical, and quantum properties.[27,28] Although, electronic structures and piezoelectric properties of two non-magnetic Janus $MSiGeN_4$ (M = Mo and W) monolayers were studied in a recent work,[29] no magnetic Janus monolayers within the same family have been predicted to date. Therefore,

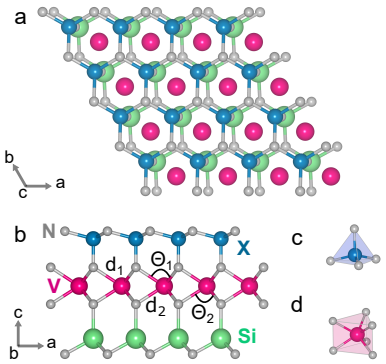

FIG. 1. (a) Top and (b) side views of the crystal structures of ternary layered $VSiXN_4$ (X = Ge, Sn) Janus monolayers. V atoms are depicted in pink, X atoms are in blue, Si atoms are in green, and N atoms are in grey. For VSi_2N_4 monolayer, X is replaced by Si. N-V-N bond angles ($\sim 90°$) and V-N bond lengths for top (bottom) layer are indicated as θ_1 (θ_2) and d_1 (d_2), respectively. The crystal field environments: (c) tetrahedral for Si/X and (d) trigonal prismatic for V atoms are shown.

here we propose two new ferromagnetic Janus monolayers, namely $VSiGeN_4$ and $VSiSnN_4$, which can be viewed as replacing one of the Si layers in VSi2N4 monolayer with Ge or Sn (Fig. 1). We demonstrate that thermodynamically stable $VSiGeN_4$ and dynamically stable $VSiSnN_4$ monolayers are weak XY-type 2D ferromagnets with transition temperatures above 300 K, and both of them are small-gap semiconductors.

Thermodynamic stability is a key property that must be addressed for new materials prediction and understanding their experimental synthesizability. It refers to the relative stability with respect to all the possible competing phases in thermodynamic equilibrium. For a material to be thermodynamically stable during growth, the chemical potentials of its constituent elements must satisfy a set of conditions. Taking $MoSi_2N_4$ as an example, one condition is that

$$\Delta\mu_{\rm Mo} + 2\Delta\mu_{\rm Si} + 4\Delta\mu_{\rm N} = \Delta H_f(MoSi_2N_4), \quad (1)$$

where $\Delta H_f(MoSi_2N_4)$ is the enthalpy of formation, which can be calculated from first-principles. $\Delta\mu_{\rm Mo}$, $\Delta\mu_{\rm Si}$, and $\Delta\mu_{\rm N}$ are the relative chemical potentials of elemental Mo, Si, and N with respect to their solid bulk components (extreme rich limits), respectively. These chemical potentials depend on the experimental growth conditions and are regarded as variable in the formalism. They are further bound by (i) the values that will cause precipitation of solid elemental Mo, Si, and N, so that

$$\Delta\mu_{\rm Mo} \le 0,\ \Delta\mu_{\rm Si} \le 0,\ \Delta\mu_{\rm N} \le 0, \quad (2)$$

and (ii) by the values that will lead to the precipitation of competing binary phases MoN and Si_3N_4, so that

$$\Delta\mu_{\rm Mo} + \Delta\mu_{\rm N} < \Delta H_f(MoN), \quad (3)$$
$$3\Delta\mu_{\rm Si} + 4\Delta\mu_{\rm N} < \Delta H_f(Si_3N_4). \quad (4)$$

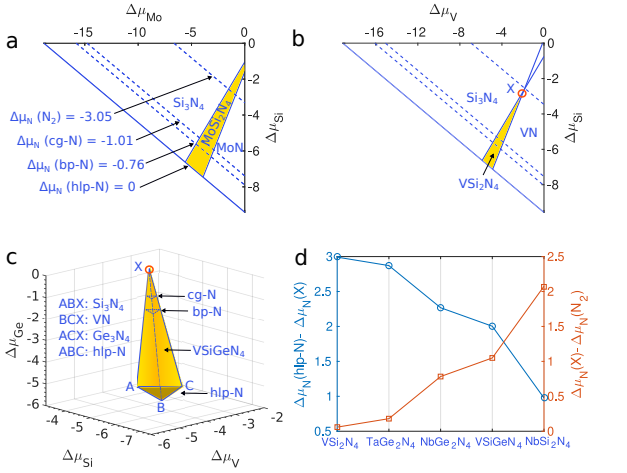

FIG. 2. 2D/3D chemical potential regions (shaded in yellow) where (a) $MoSi_2N_4$, (b) VSi_2N_4, and (c) $VSiGeN_4$ monolayers are thermodynamically stable against the formation of constituent elements and competing binary compounds. The shaded area behind the solid (dotted) blue line in the phase diagram of $MoSi_2N_4$ is the chemical potential region, where the monolayer can be synthesized using chemically rich (poor) N. X (marked in red circle) represents the vertex of the chemical potential region, up to which the respective compounds can be synthesized using chemically poor N. (d) The difference in chemical potential of N at X and N_2-gas (hlp-N) is shown in the right (left) side. All the energies are in eV.

The ranges of $\Delta\mu_{\rm Mo}$, $\Delta\mu_{\rm Si}$, and $\Delta\mu_{\rm N}$ that satisfy Eqs.1-4 define the thermodynamic stability region, where possible equilibrium experimental growth conditions are suggested. No solution to these equations means that the material investigated is thermodynamically unstable and its equilibrium experimental synthesis would be quite challenging or impossible as kinetic barriers between different phases at high temperatures are often ignorable or small.

As a test, we first perform the above thermodynamic stability analysis for two nonmagnetic monolayers $MoSi_2N_4$ and WSi_2N_4, which have been experimentally synthesized.[19] Consistent with experiment, our calculated results shown in Fig. 2a and supporting information S2(a) demonstrate that these two compounds are indeed thermodynamically stable. Their stability regions are highlighted in color yellow in the plots. Mentionably, this is defined relative to the chemical potential of hexagonal layered polymeric nitrogen (hlp-N), based on which ΔH_f are calculated. This hlp-N phase represents the extreme N-rich growth condition and was experimentally synthesized near 250 GPa.[30] The N_2 gas under normal condition is about 3.05 eV lower in chemical potential (poorer) than hlp-N; In between, there are another two metastable phases, cubic gauche polymeric nitrogen (cg-N)[31] and polymeric nitrogen allotrope with the black phosphorus structure (bp-N),[32] which were also experimentally synthesized. As displayed in Fig. 2a and supporting information S2(a), the thermodynamic stability

regions of $MoSi_2N_4$ and WSi_2N_4 both cover from extreme N-rich conditions to the conditions that are much poorer than the N_2 gas.

We now perform the same thermodynamic stability analysis for all nine magnetic MA_2Z_4 monolayers. Computational details are given in supporting information S1. Our calculated results are shown in Fig. 2b and supporting information S2(b-d). Although these monolayers were all predicted to be dynamical stable and have a negative formation enthalpy, our calculations reveal that only nitrides, except YSi_2N_4 are thermodynamically stable only under some conditions for N that are richer than N_2 gas. Their stability regions are all much narrower than $MoSi_2N_4$ and WSi_2N_4. Further, to understand the relative stability of magnetic MA_2N_4, the distance between the vertex of each chemical potential region (marked as X) and N_2 gas has been calculated. $\Delta\mu_N$(X)-$\Delta\mu_N$(N_2) increases in the order: VSi_2N_4 $\rightarrow$ $TaGe_2N_4$ $\rightarrow$ $NbGe_2N_4$ $\rightarrow$ $NbSi_2N_4$, along which the respective regions are far from the chemical potential of N_2 gas (Fig. 2d). It means that VSi_2N_4 is most stable among these magnetic nitrides. These results suggest that the experimental growth of these nitrides under thermodynamic equilibrium conditions will be difficult as extreme N-rich conditions are necessary. For VSi_2N_4, it may be grown via reaction

$$2Si_3N_4 + 3VN + N\ (\text{solid}) \longrightarrow 3VSi_2N_4. \qquad (5)$$

where solid N reactant can be hlp-N, cg-N, or bp-N. For phosphides (VSi_2P_4 and VGe_2P_4) and arsenides (VSi_2As_4 and VGe_2As_4), we cannot find any thermodynamically stable region. Thus, under equilibrium growth conditions, the competing binary phases (e.g., V_3P, VP, SiP_2, GeP_3, etc., for phosphides and V_3As, VAs, $SiAs_2$, $GeAs_2$, etc., for arsenides) of these materials would form rather than these materials themselves.

To identify more stable intrinsic ferromagnetic 2D MA_2Z_4 compounds, we extend our first-principles thermodynamic stability analysis to two novel Janus compounds, $VSiGeN_4$ and $VSiSnN_4$. They are derived from the VSi_2N_4 monolayer, which has been demonstrated thermodynmaically stable. Janus monolayers $VSiXN_4$ (X = Ge, Sn) can be viewed as a VN_2 layer sandwiched between Si-N and X-N layers (Fig. 1). Due to the presence of different group-IV elements in the top and bottom layers, such Janus monolayers lack both inversion and out-of-plane mirror symmetries in contrast to the VSi_2N_4 monolayer.

Our thermodynamic stability study reveals that both $VSiGeN_4$ and $VSiSnN_4$ monolayers have negative formation enthalpies (using hlp-N), -4.329 eV and -2.132 eV, respectively. However, only monolayer $VSiGeN_4$ is found to be thermodynamically stable. Fig. 2c shows our calculated stability region for $VSiGeN_4$ and its competing phases Si_3N_4, Ge_3N_4, and VN. As expected, this thermodynamic stability region is smaller than that of VSi_2N_4 and stays 1 eV farther from the chemical potential of N_2 gas (Fig. 2d). However, goodly, this stability region also

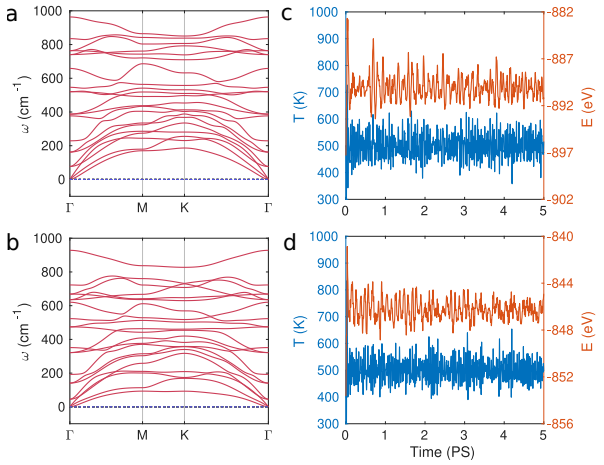

FIG. 3. (a-b) Phonon band structures, (c-d) temperatures and total energy fluctuations after 5 ps of *ab-initio* molecular dynamics simulations at 500 K of $VSiGeN_4$ (top panel) and $VSiSnN_4$ (bottom panel) Janus monolayers.

covers the chemical potentials of both cg-N and bp-N phases. The $VSiGeN_4$ monolayer may thus be synthesized via

$$Si_3N_4 + Ge_3N_4 + 3VN + \text{cg-N} \longrightarrow 3VSiGeN_4. \qquad (6)$$

For the $VSiSnN_4$ monolayer, no thermodynamic stability region is found in this study.

Both Janus monolayers $VSiGeN_4$ and $VSiSnN_4$ are also found to be dynamically and thermally stable. Fig. 3a-b show our calculated phonon spectra along the high-symmetry directions of the hexagonal Brillouin zone (BZ). No negative frequencies are found in both cases. Fig. 3c-d show our $ab-initio$ molecular dynamics simulation results for both Janus monolayers at 500 K. No indication of bond breaking or significant structural distortions is seen after 5 ps of simulation time (1 fs time step). Such stability features render these Janus materials also synthesizable using non-equilibrium techniques.[33,34]

Now, we turn to study the magnetic properties of $VSiGeN_4$ and $VSiSnN_4$ monolayers. To identify the magnetic ground state, we calculate the total energy difference between the ferromagetic (FM) and stripe antiferromagnetic (AFM) spin configurations as depicted in Fig. 4a-d using generalized gradient approximation (GGA)+U method.[35] To include correlation effects in V 3d orbitals, we choose $U = 3.2$ eV, at which the GGA+U calculated energy difference between the AFM and FM states matches with the HSE06[36] calculated one. (cf. supporting information S3.) The U value determined in this way has successfully predicted correct magnetic, structural properties in numerous systems.[37,38]

Our GGA+U calcualtions find that both Janus monolayers stabilize into a FM ground state, like VSi_2N_4 monolayer. As one can see from Table I, the FM states in $VSiGeN_4$ and $VSiSnN_4$ are 65.5 meV and 44.8 meV lower

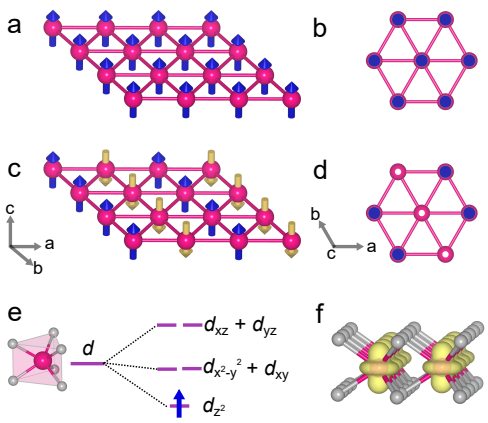

FIG. 4. Side and top views of the effective triangular lattice formed by V ions in VSi_2N_4 and $VSiXN_4$ Janus monolayers showing (a,b) FM and (c,d) stripe AFM states. V ions are shown as pink spheres. Up and down spins are indicated by blue and golden arrows. (e) A schematic of the energy levels of d orbitals in a trigonal prismatic crystal field environment. Here, only the middle layer containing V ions is displayed since the non-magnetic top and bottom layers of these monolayers do not contribute to the spin density distribution. Single valence electron of V^{4+} ion predominately occupies d_{z^2} orbital and corresponding (f) spin density distribution is shown.

Monolayer	a (Å)	E_g (eV)	m_V (μ_B)	ΔE_m (meV)	MAE (μeV)	T_{BKT} (K)
VSi_2N_4	2.90	0.50 (D)	1.10	88.7	-59	687
$VSiGeN_4$	2.97	0.48 (D)	1.11	65.5	-20	507
$VSiSnN_4$	3.07	0.85 (ID)	1.14	44.8	-10	347

TABLE I. Lattice constants (a), band gap (E_g), V magnetic moments (m_V), energy differences between the AFM and FM spin configurations (ΔE_m = (E_{AFM}-E_{FM})/f.u.), magnetic anisotropy energy (MAE), and transition temperatures (T_{BKT}) of VSi_2N_4 and $VSiXN_4$ monolayers are listed here. The band gap (E_g) values mentioned in the third column are obtained using HSE06, which agree qualitatively with the band gap values obtained within GGA+U method - VSi_2N_4: 0.3 eV (D), $VSiGeN_4$: 0.15 eV (D), $VSiSnN_4$: 0.28 eV (ID). Note, ID = Indirect and D = Direct semiconductor.

in energy than their AFM states, respectively. Magnetic moments (m_V) obtained from our GGA+U calculations agree qualitatively with the ionic description that gives a V^{4+}: $3d^1$ electronic configuration. In a trigonal prismatic crystal field environment, V d orbitals split into low-lying d_{z^2} orbital followed by (d_{xy}+$d_{x^2-y^2}$), and (d_{xz}+d_{yz}) orbitals (Fig. 4e), respectively. Our calculated spin-density distribution of occupied V d orbital (Fig. 4f) show that the top valence band in the majority-spin channel is predominantly d_{z^2} orbital character. Here, the V-N-V angle is close to 90°, and within this orthogonal setup, superexchange interaction between the V atoms mediated by the neighboring N atoms is the dominating exchange mechanism for ferromagnetism. This is in agreement with the Goodenough-Kanamori rules.[39,40] As a result, VSi_2N_4 and $VSiXN_4$ monolayers adopt a FM ordered ground state.

According to the Mermin-Wagner theorem,[41] long-range magnetic order should be absent in the 2D isotropic spin systems at any finite temperature. However, magnetic anisotropy removes this restriction and stabilizes magnetic order in 2D materials.[11,42–44] To determine the nature of magnetic anisotropy, we first calculate magnetocrystalline anisotropy (MCA) using the GGA+U method including spin-orbit coupling (SOC). MCA is defined as the energy difference between two FM spin configurations, where magnetic moments are directed along the x and z directions, respectively. For the $VSiGeN_4$ monolayer, we obtain a negative MCA (−4 μeV) and a positive MCA (4.0 μeV) for the $VSiSnN_4$ monolayer. Since MCA is significantly small here, magnetic shape anisotropy (MSA), which originated from dipole-dipole interactions may become relevant and contribute to the magnetic anisotropy energy (MAE). The calculated MSA values −17 μeV, −16 μeV, and −14 μeV for VSi_2N_4, $VSiGeN_4$, and $VSiSnN_4$ monolayers (c.f. supporting information S5 for details) are greater than the magnitude of MCA for both Janus monolayers. As a result, after the inclusion of MSA, the total MAE becomes negative (easy-plane anisotropy), and owing to its small magnitude (Table I), $VSiXN_4$ monolayers can be regarded as weak 2D-XY magnets like $CrCl_3$ monolayer.[42,45] A quasi-long-range order with a divergent correlation length could be observed below the Berezinskii-Kosterlitz-Thouless (BKT)[46] transition temperature for these planar magnets. However, due to the weak anisotropy, in-plane magnetization in both Janus monolayers could easily be tuned to out-of-plane long-range order by perturbations such as strains and defects.

The magnetic transition temperature $T_{BKT} = 1.335\ J/K_B$ is obtained from the results of the Monte Carlo simulation for 2D-XY magnets on a triangular lattice[47] (c.f. supporting information S4). We find that the transition temperature of $VSiGeN_4$ (507 K) and $VSiSnN_4$ (347 K) are lower than that of VSi_2N_4 (687 K), but they are still higher than the room temperature.

To understand the nature of MAE variations in Janus monolayers, we also calculated the MAE for strained VSi_2N_4 monolayers. Due to the presence of larger-size atoms, $VSiGeN_4$ and $VSiSnN_4$ Janus structures have their lattice constants being 2.4% and 5.8% larger than monolayer VSi_2N_4 (Table I), respectively. Fig. 5a shows the comparison of MAE values between strained monolayers VSi_2N_4 and Janus monolayers. Clearly, one can observe that the MAE values of Janus monolayers (marked as red squares) are almost identical to the MAE values of VSi_2N_4 monolayers at the same lattice constants of corresponding Janus monolayers. It means that the key factor that drives the transition from the in-plane anisotropy in VSi_2N_4 and $VSiGeN_4$ to the out-of-plane anisotropy in $VSiSnN_4$ monolayer is the biax-

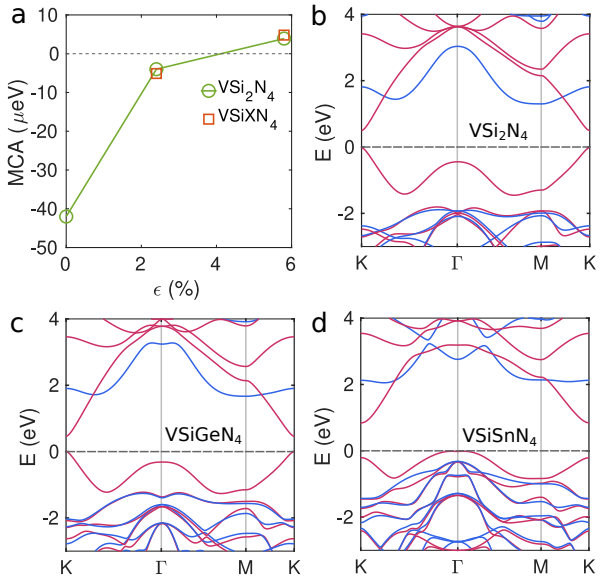

FIG. 5. (a) Comparison of magnetocrystalline anisotropy (MCA) values between strained monolayers VSi_2N_4 and Janus monolayers $VSiXN_4$ (X = Ge, Sn). ϵ is the uniform biaxial strain with respect to the VSi_2N_4 optimized lattice constant. Band structures of (b) VSi_2N_4, (c) $VSiGeN_4$, and (d) $VSiSnN_4$ monolayers within HSE method in the FM ground state. Red and blue lines in the band structures represent the majority and minority spin channels, respectively.

ial in-plane tensile strain. The strain effects of MAE in VSi_2N_4 has already been theoretically studied in past.[21] These reported results, agreeing well with ours, indicate that switching the spin anisotropy from in-plane to out-of-plane in VSi_2N_4 needs more than 4% of biaxial strains, which would be very challenging for experimental realization and disadvantageous for device applications. Here our results demonstrate that Janus engineering is an useful (and probably more viable) method to tune MAE and other properties of interest.

In addition to remarkable stability and magnetic properties, these two Janus monolayers exhibit excellent electronic properties. Fig. 5b-d depict the electronic band structures of VSi_2N_4 and $VSiXN_4$ monolayers as obtained from HSE06. VSi_2N_4 and $VSiGeN_4$ monolayers are direct-gap semiconductors with band gap (E_g) $\sim$ 0.5 eV. Interestingly, the nature of the band gap changes from direct to indirect with E_g increases to 0.85 eV for $VSiSnN_4$. This band gap switching and different E_g values make $VSiXN_4$ monolayers suitable candidates to operate at variable voltages, frequencies, and temperature range for device applications. Note that, these band structures are consistent with GGA+U method (supporting information S7).

Finally, we shed light on the valley polarization, which is the measure of spin-valley coupling. This quantity can be estimated from the energy difference (ΔE_{sv}) between valance band maxima at $-$K and +K points. For this purpose, we calculate the band structures within GGA+U+SOC (see supporting information S8) with the magnetization direction along +x and +z directions, respectively. A relatively large valley polarization of 64 meV can be induced in for VSi_2N_4 monolayer by changing the spin directions from +x to +z, consistent with the previous report.[21] However, $VSiXN_4$ monolayers have less significant contribution to the spin-valley coupling because of their very small MAE values, and thus, the valley degeneracy remains preserved.

In conclusion, through the first-principles analysis, we have shown that among all dynamically stable magnetic MA_2Z_4 monolayers, only four magnetic nitrides are thermodynamically stable under some experimentally challenging growth conditions. In the group of 2D magnetic nitrides, VSi_2N_4 has been found to be the most stable monolayer, and from which, two novel Janus ferromagnetic monolayers namely $VSiGeN_4$ and $VSiSnN_4$ have been designed. Dynamical and thermal stability of these Janus monolayers ensure their non-equilibrium growth. Alternatively, thermodynamically stable $VSiGeN_4$ monolayer, can be synthesized in an equilibrium conditions. The electronic structures reveal that they are narrow band gap semiconductors. However, the most exciting features of $VSiGeN_4$ and $VSiSnN_4$ monolayers are their weak easy-plane magnetic anisotropy, which is primarily associated with the MSA and the contrasting semiconducting nature (direct vs indirect). The novel magnetic properties of these 2D ternary layered vanadium-based Janus semiconductors make them emerging candidates for spintronics and optoelectronics applications. Besides, there is a possibility that they can host skyrmions like other Janus monolayers as reported in the contemporary literature.[48,49] These results will provide a guidance for new experimental as well as theoretical explorations on the magnetic monolayers of the MA_2Z_4 family and two novel Janus $VSiXN_4$ monolayers.

This work has been supported by the U.S. DOE, Office of Science, Office of Basic Energy Sciences, under Award Number DE-SC0021127. D.D. thanks Harrison LaBollita for the useful discussion on MSA calculations. D.D. and L.Y. gratefully acknowledge the assistance of the Advanced Computing Group of the University of Maine System for providing computational resources for this work.

* Both authors contributed equally.; dibyendu.dey@maine.edu
† Both authors contributed equally.
‡ liping.yu@maine.edu

[1] Y. Deng, Y. Yu, Y. Song, J. Zhang, N. Z. Wang, Z. Sun, Y. Yi, Y. Z. Wu, S. Wu, J. Zhu, J. Wang, X. H. Chen, and Y. Zhang, Nature **563**, 94 (2018).
[2] M. Gibertini, M. Koperski, A. F. Morpurgo, and K. S.

Novoselov, Nature Nanotechnology **14**, 408 (2019).

[3] B. Huang, G. Clark, D. R. Klein, D. MacNeill, E. Navarro-Moratalla, K. L. Seyler, N. Wilson, M. A. McGuire, D. H. Cobden, D. Xiao, W. Yao, P. Jarillo-Herrero, and X. Xu, Nature Nanotechnology **13**, 544 (2018).

[4] K. S. Burch, Nature Nanotechnology **13**, 532 (2018).

[5] R. Chua, J. Yang, X. He, X. Yu, W. Yu, F. Bussolotti, P. K. J. Wong, K. P. Loh, M. B. H. Breese, K. E. J. Goh, Y. L. Huang, and A. T. S. Wee, Advanced Materials **32**, 2000693 (2020).

[6] Y. Zhao, L. Lin, Q. Zhou, Y. Li, S. Yuan, Q. Chen, S. Dong, and J. Wang, Nano Letters **18**, 2943 (2018).

[7] S. Jiang, H. Xie, J. Shan, and K. F. Mak, Nature Materials **19**, 1295 (2020).

[8] Y. Tian, W. Gao, E. A. Henriksen, J. R. Chelikowsky, and L. Yang, Nano Letters **19**, 7673 (2019).

[9] M. Blei, J. L. Lado, Q. Song, D. Dey, O. Erten, V. Pardo, R. Comin, S. Tongay, and A. S. Botana, Applied Physics Reviews **8**, 021301 (2021).

[10] X. Jiang, Q. Liu, J. Xing, N. Liu, Y. Guo, Z. Liu, and J. Zhao, Applied Physics Reviews **8**, 031305 (2021).

[11] B. Huang, G. Clark, E. Navarro-Moratalla, D. R. Klein, R. Cheng, K. L. Seyler, D. Zhong, E. Schmidgall, M. A. McGuire, D. H. Cobden, W. Yao, D. Xiao, P. Jarillo-Herrero, and X. Xu, Nature **546**, 270 (2017).

[12] Z. Zhang, J. Shang, C. Jiang, A. Rasmita, W. Gao, and T. Yu, Nano Letters **19**, 3138 (2019).

[13] J.-U. Lee, S. Lee, J. H. Ryoo, S. Kang, T. Y. Kim, P. Kim, C.-H. Park, J.-G. Park, and H. Cheong, Nano Letters **16**, 7433 (2016).

[14] B. Anasori, Y. Xie, M. Beidaghi, J. Lu, B. C. Hosler, L. Hultman, P. R. C. Kent, Y. Gogotsi, and M. W. Barsoum, ACS Nano **9**, 9507 (2015).

[15] N. C. Frey, H. Kumar, B. Anasori, Y. Gogotsi, and V. B. Shenoy, ACS Nano **12**, 6319 (2018).

[16] D. Shcherbakov, P. Stepanov, D. Weber, Y. Wang, J. Hu, Y. Zhu, K. Watanabe, T. Taniguchi, Z. Mao, W. Windl, J. Goldberger, M. Bockrath, and C. N. Lau, Nano Letters **18**, 4214 (2018).

[17] C. J. Zhang, S. Pinilla, N. McEvoy, C. P. Cullen, B. Anasori, E. Long, S.-H. Park, A. Seral-Ascaso, A. Shmeliov, D. Krishnan, C. Morant, X. Liu, G. S. Duesberg, Y. Gogotsi, and V. Nicolosi, Chemistry of Materials **29**, 4848 (2017).

[18] L. Wang, Y. Shi, M. Liu, A. Zhang, Y.-L. Hong, R. Li, Q. Gao, M. Chen, W. Ren, H.-M. Cheng, Y. Li, and X.-Q. Chen, Nature Communications **12**, 2361 (2021).

[19] Y.-L. Hong, Z. Liu, L. Wang, T. Zhou, W. Ma, C. Xu, S. Feng, L. Chen, M.-L. Chen, D.-M. Sun, X.-Q. Chen, H.-M. Cheng, and W. Ren, Science **369**, 670 (2020).

[20] Y. Ding and Y. Wang, The Journal of Physical Chemistry C **125**, 19580 (2021).

[21] Q. Cui, Y. Zhu, J. Liang, P. Cui, and H. Yang, Phys. Rev. B **103**, 085421 (2021).

[22] X. Feng, X. Xu, Z. He, R. Peng, Y. Dai, B. Huang, and Y. Ma, Phys. Rev. B **104**, 075421 (2021).

[23] L. Yan, B.-T. Wang, X. Huang, Q. Li, K. Xue, J. Zhang, W. Ren, and L. Zhou, Nanoscale **13**, 18947 (2021).

[24] Y. Liu, Y. Ji, and Y. Li, The Journal of Physical Chemistry Letters **12**, 9149 (2021).

[25] Y. Chen, S. Tian, and Q. Tang, The Journal of Physical Chemistry C **125**, 22581 (2021).

[26] M. R. K. Akanda and R. K. Lake, Applied Physics Letters **119**, 052402 (2021).

[27] M. Yagmurcukardes, Y. Qin, S. Ozen, M. Sayyad, F. M. Peeters, S. Tongay, and H. Sahin, Applied Physics Reviews **7**, 011311 (2020).

[28] M. J. Varjovi, M. Yagmurcukardes, F. M. Peeters, and E. Durgun, Phys. Rev. B **103**, 195438 (2021).

[29] S.-D. Guo, W.-Q. Mu, Y.-T. Zhu, R.-Y. Han, and W.-C. Ren, J. Mater. Chem. C **9**, 2464 (2021).

[30] D. Laniel, G. Geneste, G. Weck, M. Mezouar, and P. Loubeyre, Phys. Rev. Lett. **122**, 066001 (2019).

[31] E. M. Benchafia, Z. Yao, G. Yuan, T. Chou, H. Piao, X. Wang, and Z. Iqbal, Nature Communications **8**, 930 (2017).

[32] D. Laniel, B. Winkler, T. Fedotenko, A. Pakhomova, S. Chariton, V. Milman, V. Prakapenka, L. Dubrovinsky, and N. Dubrovinskaia, Phys. Rev. Lett. **124**, 216001 (2020).

[33] A.-Y. Lu, H. Zhu, J. Xiao, C.-P. Chuu, Y. Han, M.-H. Chiu, C.-C. Cheng, C.-W. Yang, K.-H. Wei, Y. Yang, Y. Wang, D. Sokaras, D. Nordlund, P. Yang, D. A. Muller, M.-Y. Chou, X. Zhang, and L.-J. Li, Nature Nanotechnology **12**, 744 (2017).

[34] Y. Qin, M. Sayyad, A. R.-P. Montblanch, M. S. G. Feuer, D. Dey, M. Blei, R. Sailus, D. M. Kara, Y. Shen, S. Yang, A. S. Botana, M. Atature, and S. Tongay, Advanced Materials **34**, 2106222 (2022).

[35] S. L. Dudarev, G. A. Botton, S. Y. Savrasov, C. J. Humphreys, and A. P. Sutton, Phys. Rev. B **57**, 1505 (1998).

[36] J. Heyd, G. E. Scuseria, and M. Ernzerhof, The Journal of Chemical Physics **118**, 8207 (2003).

[37] J. Hong, A. Stroppa, J. Íñiguez, S. Picozzi, and D. Vanderbilt, Phys. Rev. B **85**, 054417 (2012).

[38] H. L. Zhuang and R. G. Hennig, Phys. Rev. B **93**, 054429 (2016).

[39] J. B. Goodenough, Phys. Rev. **100**, 564 (1955).

[40] J. Kanamori, Journal of Physics and Chemistry of Solids **10**, 87 (1959).

[41] N. D. Mermin and H. Wagner, Phys. Rev. Lett. **17**, 1133 (1966).

[42] H. H. Kim, B. Yang, S. Li, S. Jiang, C. Jin, Z. Tao, G. Nichols, F. Sfigakis, S. Zhong, C. Li, S. Tian, D. G. Cory, G.-X. Miao, J. Shan, K. F. Mak, H. Lei, K. Sun, L. Zhao, and A. W. Tsen, Proceedings of the National Academy of Sciences **116**, 11131 (2019).

[43] X. Cai, T. Song, N. P. Wilson, G. Clark, M. He, X. Zhang, T. Taniguchi, K. Watanabe, W. Yao, D. Xiao, M. A. McGuire, D. H. Cobden, and X. Xu, Nano Letters **19**, 3993 (2019).

[44] Q. Liu, L. Wang, Y. Fu, X. Zhang, L. Huang, H. Su, J. Lin, X. Chen, D. Yu, X. Cui, J.-W. Mei, and J.-F. Dai, Phys. Rev. B **103**, 235411 (2021).

[45] M. Akram, H. LaBollita, D. Dey, J. Kapeghian, O. Erten, and A. S. Botana, Nano Letters **21**, 6633 (2021).

[46] J. M. Kosterlitz and D. J. Thouless, Journal of Physics C: Solid State Physics **6**, 1181 (1973).

[47] S. Zhang, R. Xu, W. Duan, and X. Zou, Advanced Functional Materials **29**, 1808380 (2019).

[48] J. Liang, W. Wang, H. Du, A. Hallal, K. Garcia, M. Chshiev, A. Fert, and H. Yang, Phys. Rev. B **101**, 184401 (2020).

[49] C. Xu, J. Feng, S. Prokhorenko, Y. Nahas, H. Xiang, and L. Bellaiche, Phys. Rev. B **101**, 060404 (2020).